

# Zr-based bulk metallic glass clamp cell for high-pressure inelastic neutron scattering

S. Hayashida<sup>a</sup>, T. Wada<sup>b</sup>, M. Ishikado<sup>a</sup>, K. Munakata<sup>a</sup>, K. Iida<sup>a</sup>, K. Kamazawa<sup>a</sup>, R. Kajimoto<sup>c</sup>, Y. Inamura<sup>c</sup>, M. Nakamura<sup>c</sup>, K. Iwasa<sup>d</sup>, K. Ohoyama<sup>d</sup>, H. Kato<sup>b</sup>, H. Kira<sup>a</sup>, M. Matsuura<sup>a</sup>, and Y. Uwatoko<sup>a,e,f</sup>

<sup>a</sup>Neutron Science and Technology Center, Comprehensive Research Organization for Science and Society (CROSS), Tokai, Ibaraki 319-1106, Japan; <sup>b</sup>Institute for Materials Research, Tohoku University, Katahira 2-1-1, Aobaku, Sendai 980-8577, Japan; <sup>c</sup>Materials and Life Science Division, J-PARC Center, Japan Atomic Energy Agency (JAEA), Tokai, Ibaraki 319-1195, Japan; <sup>d</sup>Research and Education Center for Atomic Sciences and Graduate School of Science and Engineering, Ibaraki University, Tokai, Ibaraki 319-1106, Japan; <sup>e</sup>Faculty of Science and Engineering, Tokyo City University, 1-28-1 Tamazutsumi, Setagaya, Tokyo 158-8557, Japan; <sup>f</sup>Department of Advanced Materials Science, The University of Tokyo, Kashiwa, Chiba 277-8561, Japan

## ARTICLE HISTORY

Compiled February 17, 2026

## ABSTRACT

We report the fabrication and characterization of a Zr-based bulk metallic glass (Zr-BMG) clamp cell designed for high-pressure inelastic neutron scattering (INS) measurements. The INS spectra of the empty cell exhibit broad and featureless backgrounds, reflecting the amorphous structure of the Zr-BMG. Test measurements using a reference sample,  $\text{CsFeCl}_3$ , confirm that the neutron transmission of the Zr-BMG cell is significantly higher than that of a conventional monobloc CuBe clamp cell. These results demonstrate that the Zr-BMG clamp cell provides both enhanced neutron transparency and a clean background profile, thereby advancing high-pressure INS studies.

## KEYWORDS

Neutron scattering; bulk metallic glass; piston-cylinder clamp cell

## 1. Introduction

High-pressure inelastic neutron scattering (INS) is a powerful spectroscopic technique [1–3] that directly probes elementary excitations driven by pressures across a broad range of momentum and energy transfers. This capability provides deep insight into fundamental interactions governing pressure-induced physical phenomena. However, implementing INS under high pressure presents significant technical challenges. In general, INS measurements require relatively large sample volumes because of their weak signals. This in turn necessitates the use of bulky pressure cells, such as Paris–Edinburgh (PE) presses [4–6] and McWhan cells [7]. Although successful INS studies using these cells were reported [8–10], their large size imposes major limita-

tions, particularly in terms of neutron transmission and background scattering. Herein, piston-cylinder clamp cells have been developed for high-pressure INS experiments [11–14], and widely used to date [15–17]. The clamp cells offer a simple design, moderate pressure range (< 3 GPa), and a relatively large sample capacity.

Despite their widespread use, conventional cell materials such as CuBe and NiCrAl alloys still inherently degrade data quality due to their low neutron transmission and substantial background scattering [18]. For example, CuBe alloys exhibit a neutron transmission of only 36% at a neutron energy of 10 meV for a 1 cm path length [13], accompanied by complex background features arising mainly from phonon modes in the inelastic scattering regime [18]. NiCrAl alloys provide even lower neutron transmission, along with the phonon background. These issues hinder advancing high-pressure INS studies and strongly motivate the further development of pressure cells with improved neutron transparency and background scattering.

A major breakthrough has been achieved with the introduction of Zr-based bulk metallic glass (Zr-BMG) [19] as a pressure-cell material [20]. Zr-BMG exhibits exceptional tensile strength, and its neutron transmission (67% at 10 meV with 1 cm thickness [20]) is higher than conventional Cu- and Ni-based alloys. Moreover, Zr-BMG is nonmagnetic, comparable to CuBe alloys [20]. Most notably, its amorphous structure eliminates sharp Bragg reflections and acoustic phonons, resulting in a cleaner background in neutron scattering measurements. Indeed, Zr-BMG piston-cylinder clamp cells have already been demonstrated to be highly effective for neutron diffraction experiments [21–26]. Thus, applying Zr-BMG cell to INS experiments could offer significant advantages for investigating elementary excitations under pressure.

In this study, we present the development of a Zr-BMG piston-cylinder clamp cell specifically designed for INS measurements. Background and test-sample measurements using the designed pressure cell demonstrate its superior performance compared with the conventional CuBe-based clamp cells.

## 2. Experimental details

A schematic of the piston-cylinder clamp cell is shown in Fig. 1. Since the synthesizable size of Zr-BMG rods is limited by the critical diameter for glass formation, a hybrid-cylinder cell was adopted instead of a monobloc cell. The inner sleeve is fabricated from Zr-BMG (composition Zr<sub>55</sub>Al<sub>10</sub>Ni<sub>5</sub>Cu<sub>30</sub>), while the outer body is made of an aluminum alloy (A7075) for minimizing neutron absorption. The Zr-BMG rods with a diameter of 20 mm were synthesized using an arc-melting casting furnace. For assembly, the interface between the inner sleeve and the outer body was slightly tapered to enable shrink fitting and ensure mechanical stability under load. The diameter of the inner of the Zr-BMG cylinder is 6 mm. The wall ratio of the outer/inner radii of the Zr-BMG cylinder is 3.3, potentially yielding pressure of approximately 2 GPa [20]. In practice, the cell was confirmed to remain stable under applied pressures above 1 GPa (Appendix A). The cell was also verified to reach temperatures of 300 mK (<sup>3</sup>He refrigerator) and 170 mK (<sup>3</sup>He–<sup>4</sup>He dilution refrigerator). In addition, we confirmed that the magnetic susceptibility of the synthesized Zr-BMG is comparable to that reported previously [20].

Samples are enclosed in a polytetrafluoroethylene (PTFE) capsule with an inner diameter of 5 mm and a length of 23.5 mm. Taking into account capsule compression under pressure, the effective sample volume is approximately 190 mm<sup>3</sup>, corresponding to sample dimensions of 4.5 mm in diameter and 12 mm in length. To suppress

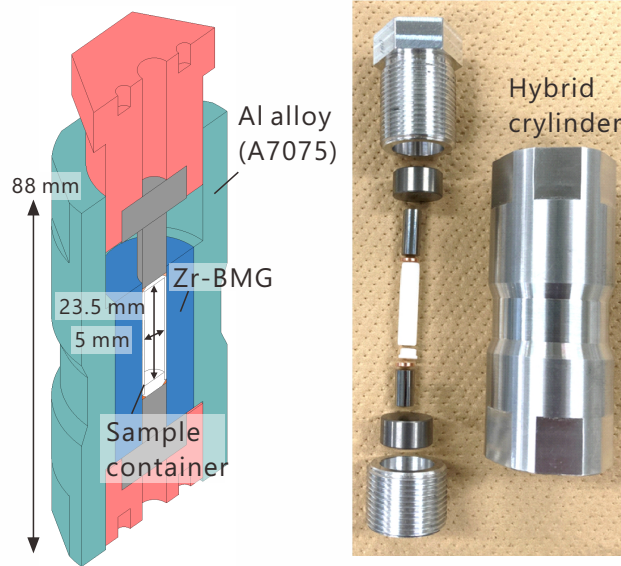


**Figure 1.** Schematic view and photograph of the full assembled hybrid cylinder clamp cell used in the present study. The blue, green and gray components correspond to the Zr-BMG inner sleeve, the aluminum alloy (A7075) outer body, and the tungsten carbide piston and support spacers, respectively. The red components are the locking nuts fabricated from either aluminum alloy or CuBe alloy.

background scattering during neutron scattering measurements, cadmium sheets were placed over the top and bottom edges of the pressure cell.

The INS measurements were carried out on the time-of-flight neutron spectrometer 4SEASONS [27] installed at Material and Life Science Facility (MLF), Japan Proton Accelerator Research Complex (J-PARC), Japan. A Fermi chopper frequency of 150 Hz was employed, providing incident neutron energies of  $E_i = 2.96, 10.2, 20.0$ , and 55.6 meV, simultaneously. An oscillating radial collimator was installed to reduce background scattering from sample environment.

A closed-cycle cryostat was used to achieve temperatures in the range of  $6 \leq T \leq 300$  K. A Zr-BMG rod with a diameter of 15 mm and a length exceeding 40 mm was measured at room temperature. The Zr-BMG hybrid cell was measured after cooling to 6 K. Test measurements were conducted using a  $\text{CsFeCl}_3$  single-crystal sample, grown by the vertical Bridgman method. The details of the synthesis procedure are described in Ref. [28]. A crystal with dimensions of approximately  $2.5 \times 3 \times 8$  mm $^3$  (mass: 260 mg) was used in this study. For the INS measurements, the scattering plane was chosen such that the crystallographic *ab*-plane was horizontal. The sample was cooled to 6 K using the closed-cycle cryostat. Measurements were first performed with the sample mounted on an aluminum plate, and subsequently repeated with the same sample placed inside the pressure cell filled with deuterated glycerol as the pressure medium. In both cases, the sample was rotated over  $62^\circ$  in  $1^\circ$  increment, with each scan lasting 11 minutes.

Data reduction for all the collected INS spectra was performed using Utsusemi software [29], and INS data were analyzed using HORACE software [30].

### 3. Results and discussion

#### 3.1. INS on Zr-BMG rod

The INS spectrum of the Zr-BMG rod is shown Fig. 2(a). In contrast to sharp acoustic phonon features observed in CuBe, NiCrAl, and aluminum alloys [18], the INS spectrum of the Zr-BMG is notably broad, characteristic of an amorphous structure. At the elastic line, a diffuse peak appears near  $Q = 2.6 \text{ \AA}^{-1}$  [Fig. 2(b)], corresponding to the conventional first sharp diffraction peak of the glass state. This is in agreement with the previous report [20]. In the inelastic regime, a broad spectrum rising from  $Q = 2.6 \text{ \AA}^{-1}$  is observed. Its intensity enhances for larger momentum transfers, exhibiting an acoustic phonon-like  $Q$  dependence governed by phonon polarization factors. This behavior indicates that the observed intensities likely originate from collective atomic vibrations. A slight enhancement of the intensity below  $Q = 2 \text{ \AA}^{-1}$  is possibly associated with atomic short-range correlations in the alloy. In the low- $Q$  regime, a broad peak is observed near 5 meV [see Fig. 2(c)], which can be attributed to a boson peak arising from low-frequency vibrational modes commonly found in glassy materials [31–33]. Unlike the sharp phonon features in the commonly used alloys [18], which complicate the extraction of sample signals, the broad features in the Zr-BMG is expected to be advantageous for separating sample signals from background scattering in high-pressure INS experiments.

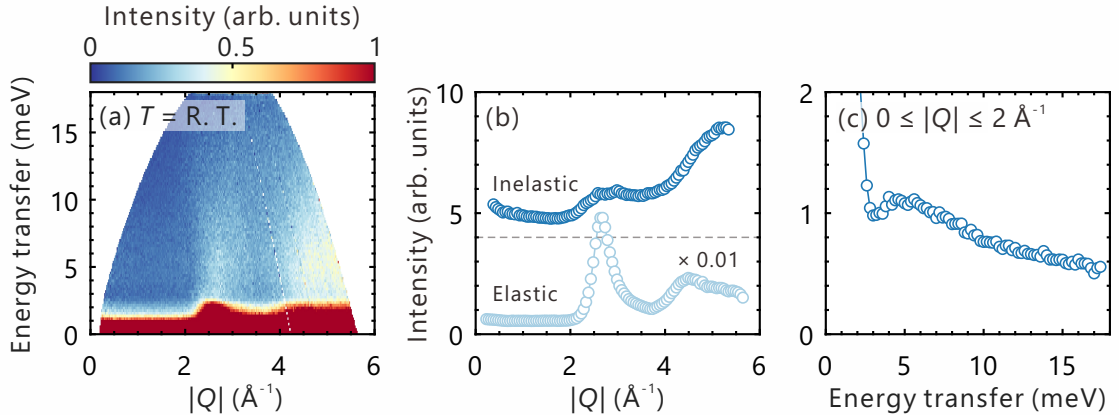


**Figure 2.** (a) False-color plot of the INS spectra of the Zr-BMG measured with  $E_i = 20.0 \text{ meV}$  at room temperature (R.T.). (b) Momentum-transfer profiles of the spectra at the elastic line integrated over  $-0.5 \leq E \leq 0.5 \text{ meV}$  and the inelastic regime integrated over  $4 \leq E \leq 16 \text{ meV}$ . For visibility, the elastic profile is scaled by a factor of 0.01, and the inelastic profile is vertically offset by 4. (c) Energy-transfer profile of the INS intensity integrated below  $2 \text{ \AA}^{-1}$ .

#### 3.2. Empty cell INS background

INS spectra of the empty pressure cell, without a sample or pressure medium, were measured at 6 K and room temperature using several incident energies up to 55.6 meV. Representative spectra are displayed in Fig. 3. Broad acoustic phonon-like spectrum, consistent with the INS spectrum of the Zr-BMG rod [Fig. 1(b)], is observed at momentum transfers above  $Q = 2.6 \text{ \AA}^{-1}$ . In addition, pronounced optical-phonon-like intensity appears around 20 meV, extending up to approximately 40 meV [Figs. 3(e) and 3(f)]. A weak feature is also visible near  $Q = 1.15 \text{ \AA}^{-1}$  at room temperature

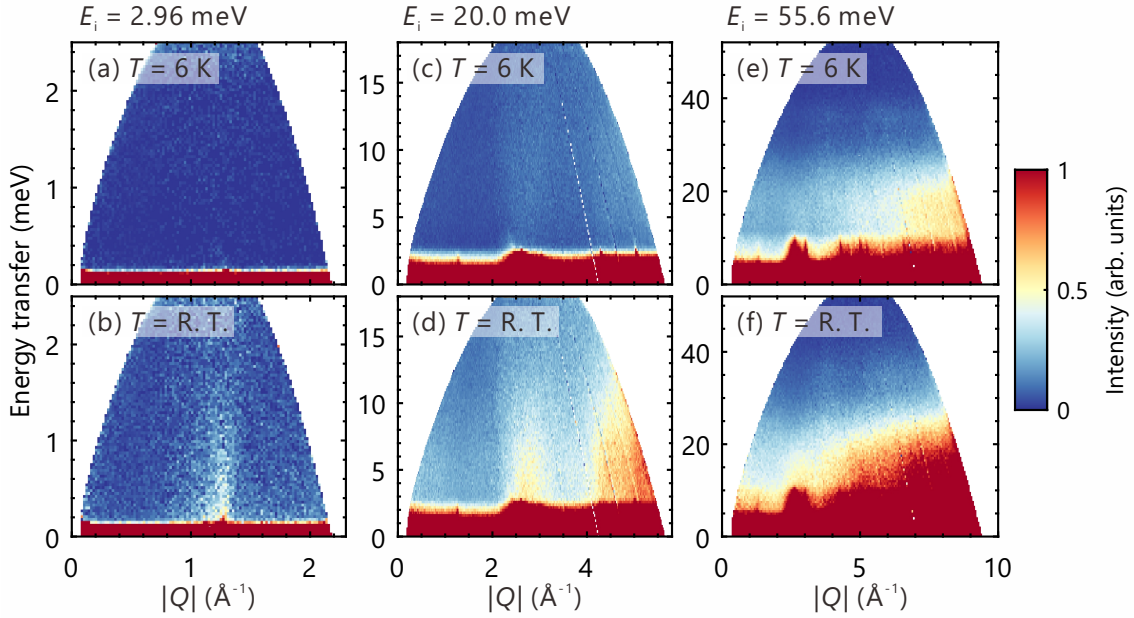


**Figure 3.** False-color plots of the INS spectra of the empty pressure cell measured with (a),(b)  $E_i = 2.96$  meV, (c),(d)  $E_i = 20.0$  meV, and (e),(f)  $E_i = 55.6$  meV. Data were taken at  $T = 6$  K (upper panels) and at room temperature (R.T., lower panels).

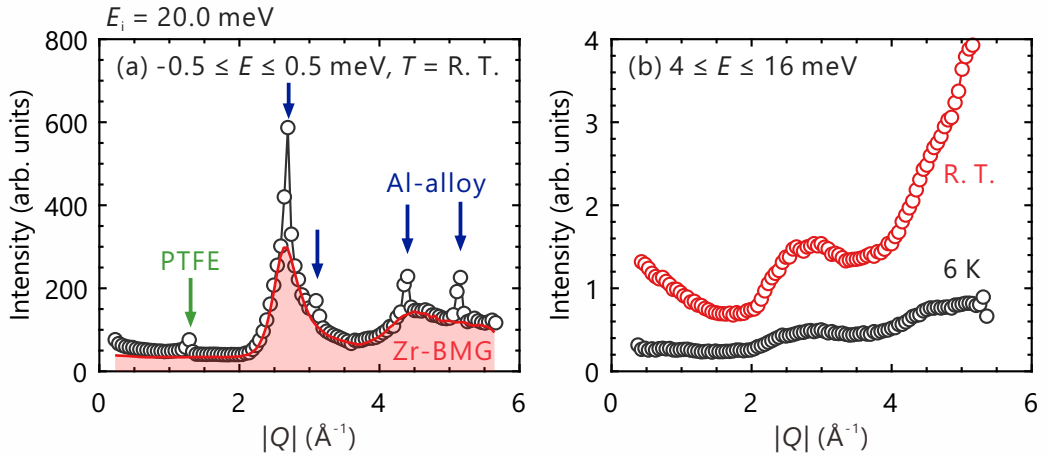


**Figure 4.** (a) Elastic line of the INS spectrum of the pressure cell (black symbols) and the Zr-BMG rod (red curve), measured at R.T. with  $E_i = 20.0$  meV. The energy transfers are integrated over  $-0.5 \leq E \leq 0.5$  meV. The intensity of the Zr-BMG rod is scaled by an arbitrary factor for visibility. Blue and green arrows indicate nuclear Bragg peaks arising from the aluminum-alloy body and the PTFE capsule, respectively. (b) Momentum-transfer profiles of the INS intensities of the cell integrated over  $4 \leq E \leq 16$  meV at  $T = 6$  K (black circles) and R.T. (red circles).

[Fig. 3(b)].

The elastic line data reveal nuclear Bragg peaks originating from the PTFE capsule [34] and the aluminum-alloy body, as indicated by the arrows in Fig. 4(a). Accordingly, the weak INS signal at  $Q = 1.15 \text{ \AA}^{-1}$  [Fig. 3(b)] is attributed to the phonon intensity from the PTFE capsule. Notably, the elastic intensities of the aluminum-alloy Bragg peaks are comparable to those of the Zr-BMG elastic scattering. This probably reflects a strong suppression of the sharp phonon intensities typically observed for

aluminum alloys [18]. Although the phonon-related features are visible in the inelastic regime at room temperature, they are significantly reduced upon cooling [Fig. 4(b)]. Consequently, the background from the Zr-BMG pressure cell is clean and featureless below  $Q = 2 \text{ \AA}^{-1}$  at low energies ( $< 10 \text{ meV}$ ), similar to that of other commonly used alloys such as CuBe and NiCrAl [18]. In high-momentum regime ( $> 2 \text{ \AA}^{-1}$ ), the background is broader than those of CuBe and NiCrAl, which is beneficial for the extraction of sample signals.

### 3.3. Test measurement on $\text{CsFeCl}_3$

To evaluate the background quality and neutron transmission of the Zr-BMG pressure cell in the low- $Q$  ( $< 2 \text{ \AA}^{-1}$ ) and low-energy ( $< 10 \text{ meV}$ ) regime, we measured INS signals of  $\text{CsFeCl}_3$  in both the bare sample and the sample enclosed in the cell. Magnetic excitations of the quantum magnet  $\text{CsFeCl}_3$ , known to exhibit a gapped dispersion relation [35], are examined under the identical measurement conditions. The INS intensities are normalized by the number of incident protons at the neutron source, enabling a direct and quantitative comparison between the two datasets. As shown in Fig. 5, the characteristic magnetic excitations, consistent with the previous studies [16,35–37], were clearly observed in both the bare sample and the sample enclosed in the cell, even though the intensity is somewhat reduced in the latter.

The reduction of the magnetic signal is estimated from a constant- $Q$  cut at  $\mathbf{Q} = (1/3, 1/3, 0)$ , as shown in Fig. 6(a). The integrated INS intensity at 0.7 meV decreases to approximately 34%. To validate this value, we calculate neutron transmission of the pressure cell materials. The transmission  $T$  is given by

$$T = \exp \left( -\frac{\rho N_A}{M} \sigma_{\text{tot}} t \right), \quad (1)$$

where  $\rho$  is the mass density of the material,  $M$  is its molar mass,  $N_A$  is the Avogadro constant, and  $t$  is the thickness of the material. The total neutron cross-section  $\sigma_{\text{tot}}$

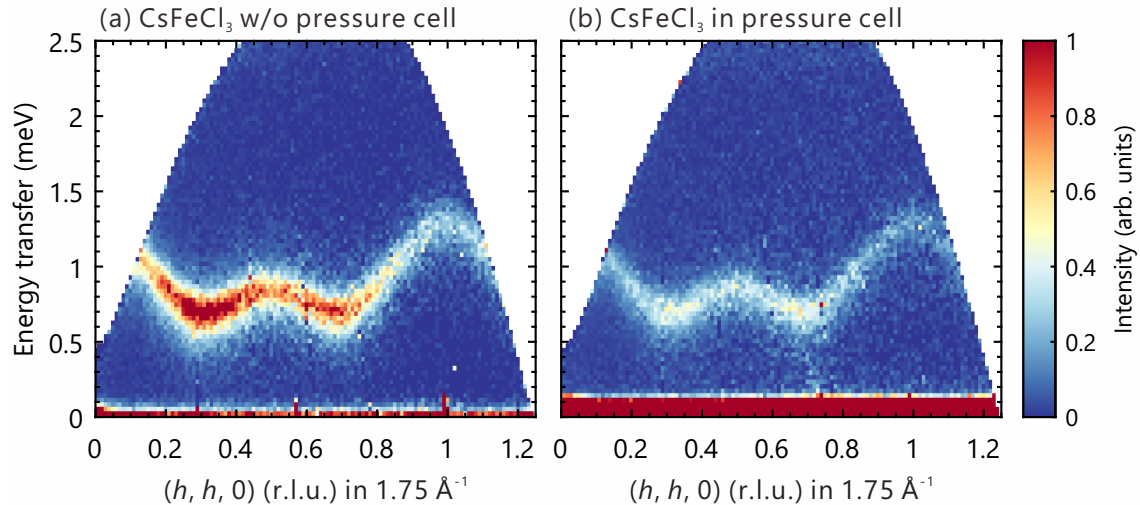


**Figure 5.** False-color plots of the INS spectra of  $\text{CsFeCl}_3$  along the [110] direction measured with  $E_i = 2.96 \text{ meV}$ . Data were collected (a) without the pressure cell and (b) with the pressure cell. The momentum transfer perpendicular to the plot axis is integrated over  $\pm 0.1 \text{ \AA}^{-1}$ .

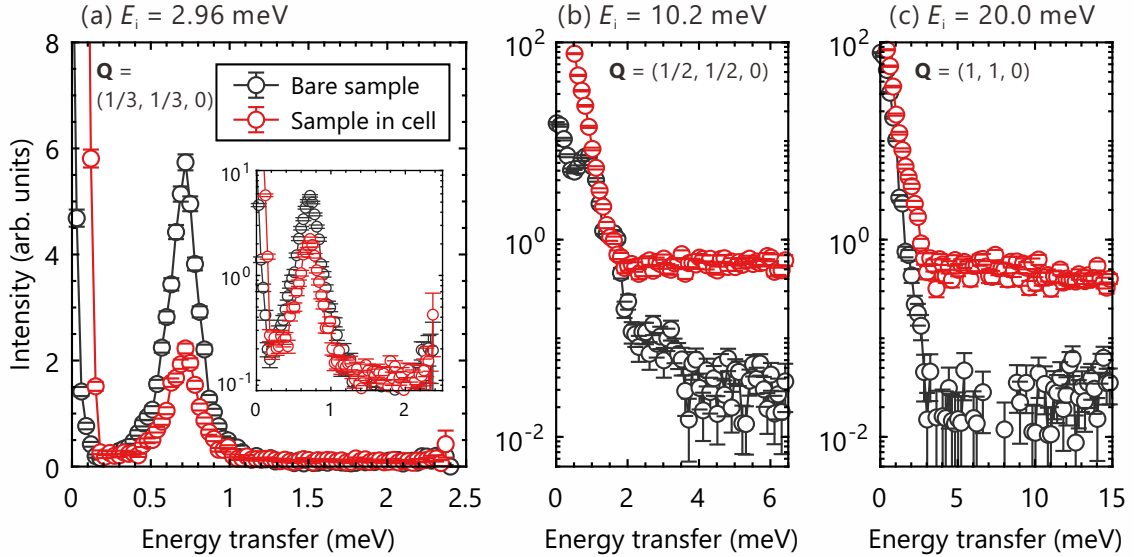


**Figure 6.** Constant- $Q$  cuts of the INS spectra of  $\text{CsFeCl}_3$  measured without and with the pressure cell for (a)  $E_i = 2.96$  meV, (b) 10.2, and (c) 20.0 meV. The cuts are taken at (a)  $\mathbf{Q} = (1/3, 1/3, 0)$ , (b)  $(1/2, 1/2, 0)$ , and (c)  $(1, 1, 0)$ , each lying below  $1.75 \text{ \AA}^{-1}$ . For  $E_i = 10.2$  and 20.0 meV, the  $\mathbf{Q}$  positions are chosen to access higher energy transfers. Momentum transfers are integrated within  $\pm 0.1 \text{ \AA}^{-1}$  along the three orthogonal directions. The inset of (a) and panels (b) and (c) are plotted on a logarithmic vertical scale.

**Table 1.** Neutron transmission ( $T$ ) at a neutron energy of 2.96 meV for the Zr-BMG and aluminum alloy, together with their material parameters: mass density  $\rho$ , molar mass  $M$ , total neutron cross-section  $\sigma_{\text{tot}}$ , and thickness  $t$ , as described in the text. The chemical composition of the aluminum alloy follow the Japanese Industrial Standard (JIS), and mass densities are given as representative values. The transmission of a monobloc CuBe cell with a thickness of 1.9 cm is taken from Ref. [13].

Material	$\rho$ (g/cm <sup>3</sup> )	$M$ (g/mol)	$\sigma_{\text{tot}}$ (b)	$t$ (cm)	$T$ (%)
$\text{Zr}_{55}\text{Al}_{10}\text{Ni}_5\text{Cu}_{30}$	6.8	748.7	117.6	1.35	42
Aluminum alloy (A7075)	2.8	26.98	2.32	1.35	81
CuBe monobloc [13]	-	-	-	1.9	13

represents the sum of the cross sections of all the elements in the materials. The values of  $\sigma_{\text{tot}}$  for each element are taken from the JENDL-4.0 neutron cross-section data library [38].  $t$  is the thickness of the material. The calculated neutron-energy dependence of the transmission is shown in Appendix B. The neutron transmission values at 2.96 meV are summarized in Table 1, with the value for the monobloc CuBe cell [13] provided for comparison. For the present Zr-BMG cell, the transmission at the energy loss of 0.7 meV with the incoming and outgoing neutrons of 2.96 and 2.26 meV is estimated to be 33%, in good agreement with the reduction extracted from the measured INS intensity. Remarkably, the transmission of the Zr-BMG cell for this neutron energy is about 2.5 times larger than that of the CuBe piston-cylinder clamp cell.

In addition to the superior transmission of the Zr-BMG cell, the Zr-BMG cell also provides a clean background in the INS spectra of samples in the cell. In the low-energy regime, as shown in the inset of Fig. 6(a), the background above 1.5 meV is nearly identical to that observed without the cell. At the higher incident energies, the background increases by roughly two orders of magnitude [Figs. 6(b) and 6(c)], yet remains featureless. This background enhancement may be attributed to atomic short-range

correlations of the alloys, the boson peak of the Zr-BMG, and incoherent scatterings from the atomic vibration within the pressure cell. Importantly, the smooth and structureless background scattering likely enables straightforward background subtraction in INS data analysis. Overall, the achievement of the high neutron transmission and clean background demonstrates that the Zr-BMG piston-cylinder clamp cell provides a clear advantage over conventional cells, such as those made of CuBe, for high-pressure INS experiments.

#### 4. Conclusions

We have developed and characterized a Zr-BMG hybrid clamp cell designed for high-pressure INS experiments. The INS data of the empty cell exhibited broad and featureless spectra, yielding a clean background profile that enhances the visibility of sample signals. Test measurements using a reference sample  $\text{CsFeCl}_3$  demonstrated that the Zr-BMG cell provided significantly higher neutron transmission than a conventional monobloc CuBe clamp cell. These results have established Zr-BMG as a highly promising alternative pressure-cell material for high-pressure INS experiments. For the future perspective, the present Zr-BMG pressure cell provides strong potential for investigating a wide range of quantum materials, including magnetic systems, quantum spin materials and unconventional superconductors.

#### Acknowledgements

We thank the sample-environment team of J-PARC-MLF for their technical supports on the cooling tests of the pressure cell. We also appreciate the assistance of K. Namba and T. Honda in the synthesis of  $\text{CsFeCl}_3$  crystals. The synthesis of Zr-BMG was conducted under GIMRT user program (Project No. 202412-RDKGE-0040), organized by Institute for Materials Research, Tohoku University. The magnetic property characterization of the synthesized Zr-BMG and the crystal growth of  $\text{CsFeCl}_3$  were carried out using a Quantum Design Magnetic Property Measurement System (MPMS) and a vertical tube furnace installed at the CROSS User Laboratory. The neutron experiments at the 4SEASONS spectrometer (J-PARC-MLF) were carried out under Proposal No. 2025C0001 (CROSS Development Use), and Proposal No. 2024I0001 and 2025I0001 (Instrument Use). Additional neutron experiment at HQR (JRR-3, JAEA) was conducted under the IRT program (Proposal No. 25412), organized by the Institute for Solid State Physics, The University of Tokyo. This study was supported in part by JSPS KAKENHI: JP23H04867 [Grant-in-Aid for Transformative Research Areas (A)] and JP24K00574 [Scientific Research (B)].

#### Appendix A. Pressure generation

The generation of pressure was examined through the variation of NaCl lattice constant obtained by neutron diffraction measurements. Neutron diffraction measurements were conducted using the high- $Q$  resolution spectrometer (HQR) installed at the T1-1 beam port of the JRR-3 research reactor, Japan Atomic Energy Agency (JAEA), Japan. A neutron wavelength of 2.46 Å was selected with a pyrolytic graphite monochromator, and the horizontal collimation sequence was Guide-40'-20'-40'. A NaCl crystal (Crystal

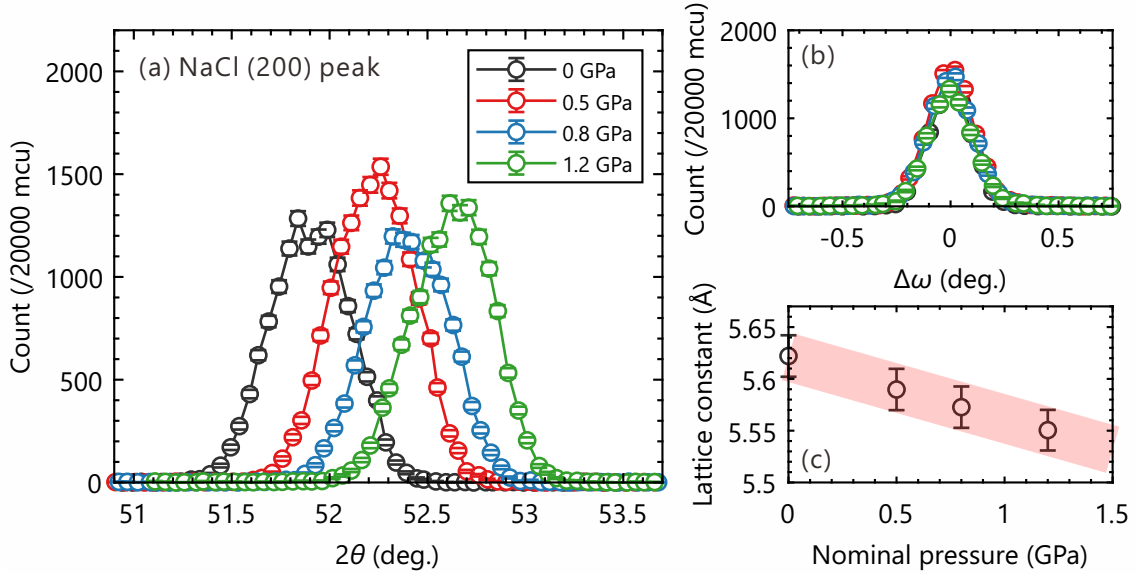


**Figure A1.** (a) Pressure dependence of  $\theta$ - $2\theta$  scans around the NaCl (200) Bragg peak. Neutron intensities are normalized to the monitor count unit (mcu). (b)  $\omega$  scans around the (200) peak at each pressure, with the peak centers nominally set to zero. (c) Pressure evolution of the NaCl lattice constant, estimated from the Gaussian function fitting of the  $\theta$ - $2\theta$  scans. Error bars are estimated from the standard deviation of the fitted Gaussian peaks. Pressures correspond to nominal values estimated from the applied load. The red thick line is a guide for the eye.

Base Co., Ltd.) with dimensions of approximately  $3.5 \times 3.5 \times 10$  mm<sup>3</sup> was placed in the pressure cell with deuterated glycerol as the pressure-transmitting medium. The crystal was aligned such that the crystallographic *ab* plane was horizontal, and the pressure cell was mounted directly on the sample stage.

Figure A1(a) shows the  $\theta$ - $2\theta$  scans around the NaCl (200) Bragg peak at various applied pressures. With increasing pressure, the Bragg peak shifts systematically toward higher angles, reflecting the compression of the NaCl lattice. Importantly, no discernible  $\theta$ - $2\theta$  peak broadening is observed, and the crystal mosaicity remains unchanged throughout the pressure range, as evidenced by the  $\omega$  scans shown in Fig. A1(b). These observations confirm that the applied pressure is essentially hydrostatic. The lattice constants, extracted from the peak positions of the  $\theta$ - $2\theta$  scans, decrease linearly with pressure [see Fig. A1(c)]. The relative volume compression of NaCl between ambient pressure and the nominal pressure of 1.2 GPa,  $(V_0 - V)/V_0$ , is estimated to be 0.0377. Using the equation of state  $V(P, T)$  for NaCl [39], the calibrated pressure is determined to be 1.0 GPa. These results demonstrate that the Zr-BMG pressure cell provides reliable and homogeneous pressurization of the sample.

## Appendix B. Simulation of neutron transmissions

Neutron transmission through materials generally depends on the energy of the incident neutrons. Figure B1 shows the neutron-energy dependence of the transmission, calculated using Eq. (1), for Zr-BMG, the aluminum alloy (A7075), the Zr-BMG hybrid pressure cell developed in this study. The energy dependence of the total cross-section  $\sigma_{\text{tot}}$  are taken from the JENDL-4.0 database [38]. Note that these transmissions do not include additional effects such as Bragg edges or phonon contributions. Notably, the

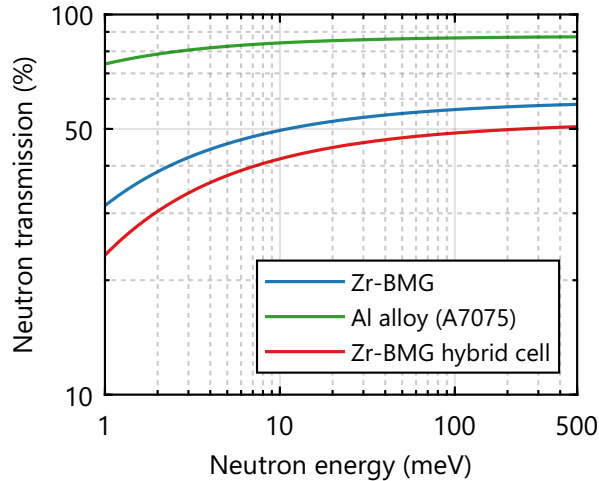


**Figure B1.** Neutron energy dependence of neutron transmission for the Zr-BMG, aluminum alloy (A7075), and Zr-BMG hybrid cell. The material thicknesses are 1.35 cm for the Zr-BMG and aluminum alloy components. The transmission of the Zr-BMG hybrid cell is calculated by combining the transmissions of the Zr-BMG and aluminum alloy.

Zr-BMG cell exhibits higher neutron transmission than the monobloc CuBe cell [13] over the entire energy range considered. In particular, its transmission exceeds that of the CuBe cell [13] by more than a factor of two below 10 meV.

## References

- [1] Somenkov VA. High-pressure neutron scattering over the ages. *Journal of Physics: Condensed Matter*. 2005 Sep;17(40):S2991. Available from: <https://doi.org/10.1088/0953-8984/17/40/001>.
- [2] Klotz S. Techniques in high pressure neutron scattering. CRC press; 2012.
- [3] Fogh E, Giri G, Gaal R, et al. Bullet pressure-cell design for neutron scattering experiments with horizontal magnetic fields and dilution temperatures. *Review of Scientific Instruments*. 2025 Apr;96(4):043902. Available from: <https://doi.org/10.1063/5.0250156>.
- [4] Besson JM, Nelmes RJ, Hamel G, et al. Neutron powder diffraction above 10 GPa. *Physica B: Condensed Matter*. 1992 Jun;180-181:907–910. Available from: <https://www.sciencedirect.com/science/article/pii/092145269290505M>.
- [5] Besson JM, Pruzan P, Klotz S, et al. Variation of interatomic distances in ice VIII to 10 GPa. *Phys Rev B*. 1994 May;49:12540–12550. Available from: <https://link.aps.org/doi/10.1103/PhysRevB.49.12540>.
- [6] Klotz S, Hamel G, Frelat J. A new type of compact large-capacity press for neutron and x-ray scattering. *High Pressure Research*. 2004 Jan;24(1):219–223. Available from: <https://doi.org/10.1080/08957950410001661963>.
- [7] McWhan DB, Bloch D, Parisot G. Apparatus for neutron diffraction at high pressure. *Review of Scientific Instruments*. 1974 May;45(5):643–646. Available from: <https://doi.org/10.1063/1.1686704>.
- [8] Hattori T, Nakamura M, Iida K, et al. Hydrogen vibration excitations of  $ZrH_{1.8}$  and  $TiH_{1.84}$  up to 21 GPa by incoherent inelastic neutron scattering. *Phys Rev B*. 2022 Oct;106:134309. Available from: <https://link.aps.org/doi/10.1103/PhysRevB.106.134309>.
- [9] Fogh E, Giri G, Zayed ME, et al. Spin Waves and Three Dimensionality in the High-

Pressure Antiferromagnetic Phase of  $\text{SrCu}_2(\text{BO}_3)_2$ . *Phys Rev Lett.* 2024 Dec;133:246702. Available from: <https://link.aps.org/doi/10.1103/PhysRevLett.133.246702>.

[10] Zayed ME, Rüegg C, Larrea J J, et al. 4-spin plaquette singlet state in the Shastry–Sutherland compound  $\text{SrCu}_2(\text{BO}_3)_2$ . *Nat Phys.* 2017 Oct;13(10):962–966. Available from: <https://doi.org/10.1038/nphys4190>.

[11] Wang W, Sokolov DA, Huxley AD, et al. Large volume high-pressure cell for inelastic neutron scattering. *Review of Scientific Instruments.* 2011 Jul;82(7):073903. Available from: <https://doi.org/10.1063/1.3608112>.

[12] Podlesnyak A, Loguillo M, Rucker GM, et al. Clamp cell with in situ pressure monitoring for low-temperature neutron scattering measurements. *High Pressure Research.* 2018 Oct; 38(4):482–492. Available from: <https://doi.org/10.1080/08957959.2018.1519560>.

[13] Hattori T, Ohira-Kawamura S, Kawasaki T. Development of a hybrid piston cylinder cell for quasielastic neutron scattering experiments up to 1 GPa. *High Pressure Research.* 2022 Apr;42(2):226–235. Available from: <https://doi.org/10.1080/08957959.2022.2068954>.

[14] Yuan B, Mole R, Wang CW, et al. Two pressure cells for quasielastic and inelastic neutron scatterings. *EPJ Web Conf.* 2022;272. Available from: <https://doi.org/10.1051/epjconf/202227202009>.

[15] Perren G, Möller JS, Hüivonen D, et al. Spin dynamics in pressure-induced magnetically ordered phases in  $(\text{C}_4\text{H}_{12}\text{N}_2)\text{Cu}_2\text{Cl}_6$ . *Phys Rev B.* 2015 Aug;92:054413. Available from: <https://link.aps.org/doi/10.1103/PhysRevB.92.054413>.

[16] Hayashida S, Matsumoto M, Hagihala M, et al. Novel excitations near quantum criticality in geometrically frustrated antiferromagnet  $\text{CsFeCl}_3$ . *Science Advances.* 2019; 5(10):eaaw5639. Available from: <https://www.science.org/doi/abs/10.1126/sciadv.aaw5639>.

[17] Hong T, Ying T, Huang Q, et al. Evidence for pressure induced unconventional quantum criticality in the coupled spin ladder antiferromagnet  $\text{C}_9\text{H}_{18}\text{N}_2\text{CuBr}_4$ . *Nat Commun.* 2022 Jun;13(1):3073. Available from: <https://doi.org/10.1038/s41467-022-30769-8>.

[18] Kibble MG, Laliena V, Goodway CM, et al. Low-background materials for high pressure cells used in inelastic neutron scattering experiments. *Journal of Neutron Research.* 2019 Jan;21(3-4):105–116. Available from: <https://doi.org/10.3233/JNR-190115>.

[19] Inoue A. Stabilization of metallic supercooled liquid and bulk amorphous alloys. *Acta Mater.* 2000 Jan;48(1):279–306. Available from: <https://www.sciencedirect.com/science/article/pii/S1359645499003006>.

[20] Komatsu K, Munakata K, Matsubayashi K, et al. Zr-based bulk metallic glass as a cylinder material for high pressure apparatuses. *High Pressure Research.* 2015 Jul;35(3):254–262. Available from: <https://doi.org/10.1080/08957959.2015.1041939>.

[21] Matsuda M, Ye F, Dissanayake SE, et al. Pressure dependence of the magnetic ground states in MnP. *Phys Rev B.* 2016 Mar;93:100405. Available from: <https://link.aps.org/doi/10.1103/PhysRevB.93.100405>.

[22] Chi S, Uwatoko Y, Cao H, et al. Magnetic Precursor of the Pressure-Induced Superconductivity in Fe-Ladder Compounds. *Phys Rev Lett.* 2016 Jul;117:047003. Available from: <https://link.aps.org/doi/10.1103/PhysRevLett.117.047003>.

[23] Matsuda M, Lin FK, Yu R, et al. Evolution of Magnetic Double Helix and Quantum Criticality near a Dome of Superconductivity in CrAs. *Phys Rev X.* 2018 Jul;8:031017. Available from: <https://link.aps.org/doi/10.1103/PhysRevX.8.031017>.

[24] Yamashita K, Komatsu K, Klotz S, et al. A nano-polycrystalline diamond anvil cell with bulk metallic glass cylinder for single-crystal neutron diffraction. *High Pressure Research.* 2020 Jan;40(1):88–95. Available from: <https://doi.org/10.1080/08957959.2019.1700980>.

[25] Dissanayake SE, Ye F, Tian W, et al. Pressure dependence of the magnetic ground state in  $\text{CePtSi}_2$ . *Phys Rev B.* 2022 Jun;105:245111. Available from: <https://link.aps.org/doi/10.1103/PhysRevB.105.245111>.

[26] Matsuda M, Cheng J, Uwatoko Y. Pressure variation of magnetism in chromium and

manganese mono-pnictide superconductors. *Journal of the Physical Society of Japan*. 2025 Mar;94(3):032001. Available from: <https://doi.org/10.7566/JPSJ.94.032001>.

- [27] Kajimoto R, Nakamura M, Inamura Y, et al. The Fermi Chopper Spectrometer 4SEASONS at J-PARC. *J Phys Soc Jpn*. 2011;80(Suppl.B):SB025. Available from: <https://doi.org/10.1143/JPSJS.80SB.SB025>.
- [28] Kurita N, Tanaka H. Magnetic-field- and pressure-induced quantum phase transition in  $\text{CsFeCl}_3$  proved via magnetization measurements. *Phys Rev B*. 2016 Sep;94:104409. Available from: <https://link.aps.org/doi/10.1103/PhysRevB.94.104409>.
- [29] Inamura Y, Nakatani T, Suzuki J, et al. Development Status of Software “Utsusemi” for Chopper Spectrometers at MLF, J-PARC. *J Phys Soc Jpn*. 2013;82(Suppl.A):SA031. Available from: <https://doi.org/10.7566/JPSJS.82SA.SA031>.
- [30] Ewings R, Buts A, Le M, et al. Horace: Software for the analysis of data from single crystal spectroscopy experiments at time-of-flight neutron instruments. *Nucl Instrum Methods Phys Res A*. 2016;834:132–142. Available from: <https://www.sciencedirect.com/science/article/pii/S016890021630777X>.
- [31] Buchenau U, Nücker N, Dianoux AJ. Neutron Scattering Study of the Low-Frequency Vibrations in Vitreous Silica. *Phys Rev Lett*. 1984 Dec;53:2316–2319. Available from: <https://link.aps.org/doi/10.1103/PhysRevLett.53.2316>.
- [32] Sette F, Krisch MH, Masciovecchio C, et al. Dynamics of glasses and glass-forming liquids studied by inelastic x-ray scattering. *Science*. 1998 Jun;280(5369):1550–1555. Available from: <https://doi.org/10.1126/science.280.5369.1550>.
- [33] Li Y, Yu P, Bai HY. Study on the boson peak in bulk metallic glasses. *Journal of Applied Physics*. 2008 Jul;104(1):013520. Available from: <https://doi.org/10.1063/1.2948926>.
- [34] Bouznik VM, Kirik SD, Solovyov LA, et al. A crystal structure of ultra-dispersed form of polytetrafluoroethylene based on X-ray powder diffraction data. *Powder Diffraction*. 2004;19(3):219–224. Available from: <https://www.cambridge.org/core/product/B8EF6FD17BE55941525C1502C473D881>.
- [35] Yoshizawa H, Kozukue W, Hirakawa K. Neutron Scattering Study of Magnetic Excitations in Pseudo-One-Dimensional Singlet Ground State Ferromagnets  $\text{CsFeCl}_3$  and  $\text{RbFeCl}_3$ . *J Phys Soc Jpn*. 1980 Jul;49(1):144–153. Available from: <https://doi.org/10.1143/JPSJ.49.144>.
- [36] Hayashida S, Stoppel L, Yan Z, et al. Chemical composition induced quantum phase transition in  $\text{Cs}_{1-x}\text{Rb}_x\text{FeCl}_3$ . *Phys Rev B*. 2019 Jun;99:224420. Available from: <https://link.aps.org/doi/10.1103/PhysRevB.99.224420>.
- [37] Stoppel L, Hayashida S, Yan Z, et al. Anomalous spin waves in  $\text{CsFeCl}_3$  and  $\text{RbFeCl}_3$ . *Phys Rev B*. 2021 Sep;104:094422. Available from: <https://link.aps.org/doi/10.1103/PhysRevB.104.094422>.
- [38] Shibata K, Iwamoto O, Nakagawa T, et al. JENDL-4.0: A New Library for Nuclear Science and Engineering. *Journal of Nuclear Science and Technology*. 2011 Jan;48(1):1–30. Available from: <https://doi.org/10.1080/18811248.2011.9711675>.
- [39] Brown JM. The NaCl pressure standard. *Journal of Applied Physics*. 1999 Nov; 86(10):5801–5808. Available from: <https://doi.org/10.1063/1.371596>.